The measurement of the surface energy of solids by sessile drop accelerometry

Alfredo Calvimontes [1]*

[1] Predevelopment, Division Dish Care, BSH Hausgeräte GmbH (a subsidiary of Robert Bosch GmbH), Robert-Bosch-Straße 16, 89407 Dillingen an der Donau, Germany

* Correspondence: alfredo.calvimontes@bshg.com; Tel.: +49-9071-52-2410

Abstract: A new method, the sessile drop accelerometry (SDACC) for the study and measurement of the interfacial energies of solid-liquid-gas systems, is tested and discussed in this study. The laboratory instrument and technique –a combination of a drop shape analyzer with high-speed camera and a laboratory drop tower- and the evaluation algorithms, were designed to calculate the interfacial energies as a function of the geometrical changes of a sessile droplet shape due to the effect of "switching off" gravity during the experiment. The method bases on the thermodynamic equilibrium of the system interfaces and not on the balance of bi-dimensional tensions on the solid-liquid-gas contour line. A comparison of the mathematical model that supports the method with the widely accepted Young`s equation is discussed in this study.

1. Background

Young [1] proposed two hundred years ago that the contact angle of the three-phase contact line results from the balance of three tensors. This idea can be expressed by the following equation:

$$\gamma_S = \gamma_{SL} + \gamma_L \cos\theta_Y \tag{1}$$

where γ_S, γ_{SL}, and γ_L represent the interfacial tensions per unit length of the solid-vapor, solid-liquid, and liquid-vapor contact line respectively, i.e. the surface tensions, and θ_Y is the contact angle.

In principle, there are three important conditions for applying Young's equation [2]: the surface has to be chemically homogeneous, completely flat and smooth, and the solid-liquid-vapor system must be free of the effects of gravity. Under these conditions, the Equation 1 represents the mechanical balance of three surface tensions along the contour line of the three phases. This balance has also been derived using the principle of minimizing the total free energy of the system [3-5]. Most recent thermodynamic derivation relies on interpreting γ_S, γ_{SL}, and γ_L as scalar thermodynamic surface energies instead of tension vectors [4].

According to Makkonen [6], a very important reason for adopting the surface energy interpretation is that, while γ_{SL} and γ_L can be interpreted either way, the surface tension on a dry solid, γ_S, is a contentious concept [3, 7-11]. Bikerman [8] and Ivanov et al. [9] have argued that Young's equation is not a balance of forces. At the same time, the surface energy interpretation has led to many misunderstandings of the wetting phenomenon on patterned surfaces [12, 13]. The validity of Young's equation was questioned [6] at the nanoscale [14-17] and on flexible surfaces [17-18] as well.

According to Leger and Joanny, [19] the effect of body forces such as gravity on the contact line is small for small drop volumes. Gravity would affect the shapes of wetting liquid drops in their central region where they are flattened, but in a small region, close to the contact line, one would expect that the liquid-vapor and liquid-solid interfaces to make an angle given by Young's law. These observations were

41 supported by the theoretical calculations of Fujii and Nakae [20]. According to Leger, Joanny, Fujii and
42 Nakae, only forces that become increasingly large at the contact line such as the viscous force on an
43 advancing liquid can affect Young's law. However, recent experimental evidence using microgravity by
44 parabolic arc flights [21] and microgravity drop towers [22-23] have demonstrated that the effect of
45 gravity on the contact angle is relevant even at very small drop volumes such as 5 μL. According to Allen
46 [24], who studied the wetting of very small drops with small contact angles, a drop is small enough to
47 neglect gravitational influences only if its volume is less than 1 μL.

48 Of the four parameters of Young's equation, only γ_L and θ_Y can be readily measured; hence, this
49 equation can only provide the difference between the solid-vapor surface tension γ_S and the solid-liquid
50 interfacial tension γ_{SL}. For this reason, an additional equation providing a relation among the surface
51 tensions in Young's equation is required, i.e.,

$$\gamma_{SL} = f\left(\gamma_S, \gamma_L\right) \tag{2}$$

52 Such an equation is referred to as an equation of state for interfacial tensions [25]. Combining
53 Equation 1 with Equation 2, yield:

$$\gamma_L \cos\theta_Y = \gamma_S - f\left(\gamma_S, \gamma_L\right) \tag{3}$$

54 This equation was the start point for several attempts to obtain mathematical expressions or
55 numerical procedures able to provide the values of γ_S and γ_{SL} when only the values of γ_L and θ_Y are known.
56 The most relevant solutions [26] were given by Fox and Zisman [27], Owens and Wendt [28], Janczuk and
57 Bialopiotrowicz [29], Wu [30], van Oss, Chaudhury and Good [31], Li and Neumann [25], Kwok et al. [32],
58 Shimizu and Demarquette [33] and Chibowski et al. [34]. Except for the Li-Neumann method, all the
59 mentioned solutions use a pair or more liquids to calculate the surface energy of the solid and the
60 interface solid-liquid. Experimental results of Hejda et al. [24] show that the solution of the mathematical
61 approaches strongly depends on the liquids used. According to these authors, the approach proposed by
62 Li and Neumann is also impractical because its strong dependence on the liquids used for the
63 calculations.

64 More recently [35], a lab-scale microgravity tower was used to calculate the surface energies by
65 means of sessile drops. This new method, the Sessile Drop Accelerometry (SDACC), revisit the
66 phenomenon of wetting paying more attention to its surface nature as much as the derived approaches of
67 Young's equation have been put in the balance on the contact line of the three phases.

2. Theoretical Fundamentals of the Method

69 The major thermodynamic quantity which characterizes a surface or an interface is the reversible
70 work, γ, to create a unit area of surface at constant temperature (T), volume (V), and chemical potential of
71 component i (μ_i). This quantity is not equal to the surface free energy except under certain conditions [36].
72 The term surface tension was used to describe the contractile nature of surface films, i.e. their tendency to
73 minimize surface area. This term became so entrenched in the literature that it is widely used today. Thus
74 γ is widely called the surface tension, though the meaning of those words may have little physical
75 significance in many situations. As mentioned above, the quantity γ is the scalar thermodynamic surface
76 energy that characterizes the thermodynamic property of an interface.

77 The γ of a newly created surface is defined as:

$$\gamma = \frac{dw}{d\Omega} \tag{4}$$

78 i.e., the specific surface work to form $d\Omega$ new surface area.

79 The thermodynamics of interfaces is the same as the thermodynamics of homogeneous systems
80 except that the work term of conventional thermodynamics must include all the $\gamma d\Omega$ components for the

81 heterogeneous (interface-containing) systems [36]. In systems where charges or electrical potentials are
82 present, the electrical work must also be included. This is usually done using the electrochemical
83 potential.
84   By open systems with surfaces, in the absence of other forms of work, e.g. electrical, magnetic,
85 gravitational, etc., the Internal Energy E can be defined as:

$$dE = T\,dS - P\,dV + \sum_i \mu_i\,dN_i + \gamma\,d\Omega \tag{5}$$

86   The Enthalpy H is:

$$dH = T\,dS - V\,dP + \sum_i \mu_i\,dN_i + \gamma\,d\Omega \tag{6}$$

87   The Helmholtz energy A is:

$$dA = -S\,dT - P\,dV + \sum_i \mu_i\,dN_i + \gamma\,d\Omega \tag{7}$$

88   And the Gibbs free energy G is:

$$dG = -S\,dT + V\,dP + \sum_i \mu_i\,dN_i + \gamma\,d\Omega \tag{8}$$

89   By these systems, the creation of a new area of surface, $d\Omega$, may cause a flow of dN molecules to or
90 from the surface region, resulting in concentration profiles [37], which lead to a surface excess (or
91 deficiency) of component i:

$$\Gamma_i = \frac{dN_i}{d\Omega} \tag{9}$$

92   As a consequence:

$$\sum_i \mu_i\,dN_i = \sum_i \mu_i\,\Gamma_i\,d\Omega \tag{10}$$

93   From basic thermodynamics, the chemical potential of component i, μ_i, is given as:

$$\mu_i = \left(\frac{\partial A}{\partial N_i}\right)_{T,V,N_j,\Omega} \tag{11}$$

94

$$\mu_i = \left(\frac{\partial G}{\partial N_i}\right)_{T,P,N_j,\Omega} \tag{12}$$

95

$$\mu_i = \left(\frac{\partial E}{\partial N_i}\right)_{S,V,N_j,\Omega} \tag{13}$$

96   Where P = Pressure, S = Entropy, N_j = the number of molecules other than type i, and Ω = the surface
97 area.
98   Using Equation 9 and applying basic thermodynamics, one can develop expressions for surface
99 energy, surface Gibbs free energy, and surface Helmholtz energy:

$$\left(dE\right)_V = T\,dS + \gamma\,d\Omega + \sum_i \mu_i\,d\Gamma_i\,d\Omega \tag{14}$$

$$\left(dA\right)_{T,V} = \gamma\,d\Omega + \sum_i \mu_i\,d\Gamma_i\,d\Omega \tag{15}$$

$$\left(dG\right)_{T,P} = \gamma\,d\Omega + \sum_i \mu_i\,d\Gamma_i\,d\Omega \tag{16}$$

The corresponding specific energy and specific free energies are:

$$\left(\frac{dE}{d\Omega}\right)_V = e_s = T\frac{dS}{d\Omega} + \gamma + \sum \mu_i\Gamma_i = specific \;\; surface \;\; energy \tag{17}$$

$$\left(\frac{dA}{d\Omega}\right)_{T,V} = a_s = \gamma + \sum \mu_i\Gamma_i = specific \;\; surface \;\; Helmholtz \;\; energy \tag{18}$$

$$\left(\frac{dG}{d\Omega}\right)_{T,P} = g_s = \gamma + \sum \mu_i\Gamma_i = specific \;\; surface \;\; Gibbs \;\; free \;\; energy \tag{19}$$

At constant T, P, S, V, and if $\Gamma_i = 0$, $\gamma = e_s = a_s = g_s$, but only under these conditions.

In general, the surface Helmholtz and Gibbs free energies and the surface "internal" energy are different quantities. Because pressure is a more constant parameter than volume in heterogeneous systems, Helmholtz energy is usually preferred over Gibbs free energy [36].

The process of forming a new surface can be divided into two parts:
1. The phase must be cleaved to expose the new surface
2. Atoms in the surface plane rearrange to assume their equilibrium positions

In a multicomponent system, part 2 may also be combined with the migration of bulk atoms to or from the interface, i.e., the development of surface excesses or deficiencies, Γ_i. In a liquid, parts 1 and 2 occur nearly instantaneously. In a solid, part 2 may occur very slowly or not at all [36].

In a one-component system, $\Gamma_i = 0$ unless there is such a stoichiometric restructuring around the interface so as to significantly change the density of the phase near the surface.

Therefore, at a constant density in a single-component system $\gamma = a_s = g_s$, or γ is both the specific Gibbs free energy and the specific Helmholtz energy. Thus, γ can be called the specific surface free energy. At constant S (no morphological restructuring), γ will also be the specific surface energy.

γ is a thermodynamic property of an interface; it is not in general g_s, a_s, or e_s, though it may be equal to one, two, or all three of these quantities under certain conditions. The specific surface work of Equation 4 is commonly called the "surface tension". For this reason, "surface tension" and "surface free energy" are synonymous with the understanding that both really are the specific surface Helmholtz energy.

On the other hand, surface stress is the work necessary to stretch or compress an existing surface. In a liquid this cannot be done without causing more atoms to join the surface; i.e., creating a new surface. Hence in liquids, the surface stress is γ_L (the reversible work to form new surface; i.e., surface tension. In a solid, this is not so because the lack of mobility of atoms means that a process can stretch them without causing bulk atoms to join the surface planes. Thus, the process may stretch or compress the surface of a

4

129   solid without changing the number of atoms in the surface, only their distances of separation, thus
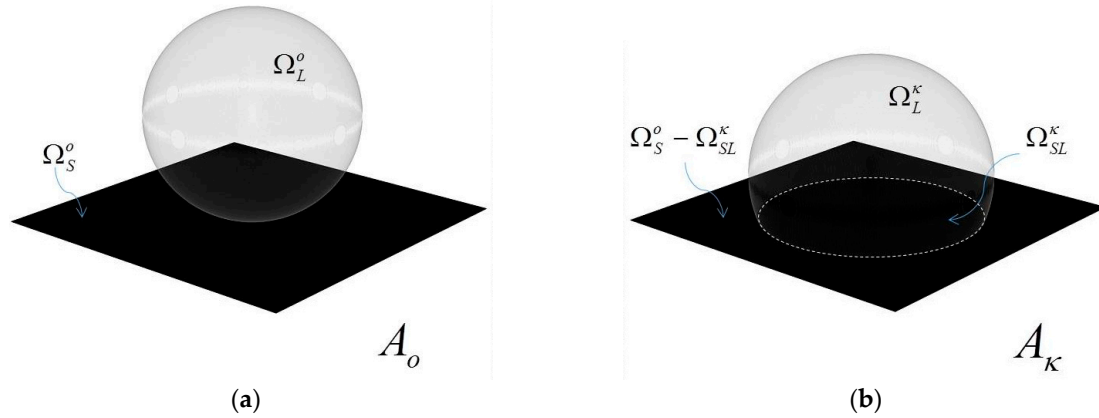130   producing a surface stress [36].
131

Figure 1. In the absence of gravity, the droplet of the state A_o (**a**) spontaneously spreads on the surface and
reaches the state A_κ (**b**).

134   Let's consider a system where, in the initial condition that we will call the configuration o, the lower
135   end of a liquid droplet is at an infinitesimal distance from a smooth solid flat surface of area $\Omega^o{}_S$ in a gas
136   medium (Figure 1a). No force field is affecting the system (the acceleration of the system is zero, i.e. $a^*=0$).
137   Due to the absence of gravity, the shape of the droplet is a perfect sphere of area $\Omega^o{}_L=4\pi r_o{}^2$, where r_o is the
138   radius of the sphere. Under these conditions, and only due to the work developed by the surface energies
139   of the system, the droplet spontaneously spreads the surface (Figure 1b) up to reach the configuration κ.
140   This results in the formation of $\Omega^\kappa{}_{SL}$, an interfacial area between the solid and the liquid. The area of a
141   perfect spherical dome formed by the interface liquid-gas is $\Omega^\kappa{}_L$.
142   A quantity of importance in this analysis, as demonstrated above, is the change –the difference- of
143   Helmholtz energy between each two contiguous j-configurations of the system during the spontaneous
144   wetting process [38]. The term "configuration" refers to a state in which the droplet is at rest in a position
145   of stable or metastable equilibrium. All the transient states among them are also thermodynamic
146   configurations. Associated with each configuration are the characteristic interfacial areas $\Omega^j{}_{SL}$, $\Omega^j{}_L$ and a
147   characteristic Helmholtz energy, A_j.
148   For a given configuration, according to the Equation 18, and at constant T, V, and if $\Gamma_i = 0$ (one-
149   component liquid, solid and gas):

$$\Delta A_j \quad = \quad \Delta\sum(\gamma\Omega)_j \quad - \quad \Delta\sum(\gamma\Omega)_i \tag{20}$$

150   Let's take as an example a system in which $\gamma_L > \gamma_{SL} > \gamma_S$. During the spontaneous wetting of the droplet
151   of Figure 1, the Helmholtz energy of the system decreases because part of the liquid-gas interface creates a
152   new solid-liquid interface (Figure 2, left). The energy of the solid-gas interface contributes additionally to
153   the creation of the solid-liquid interface. The wetting process ends when the system reaches the
154   equilibrium in the configuration κ.
155   The wetting process could end precisely at the configuration $d`$, where the Helmholtz energy of two
156   contiguous j-configurations presents no more change ($\Delta A_j = 0$). However, the internal energy stored inside
157   the drop during the wetting between o and d' can make the work necessary to continue wetting from d'
158   up to the equilibrium configuration κ, i.e., $\Delta E = A_\kappa - A_{d'}$. At this point, the configuration κ, the Helmholtz
159   energy of the system recovers the value of the initial configuration o. In other words, comparing the
160   configurations o and κ, no work has been done on the system, nor has it done any work on its
161   surroundings. The net change of Helmholtz energy during the wetting process is zero.

5

$$\Delta A_{o \to \kappa} = A_\kappa - A_o = 0 \tag{21}$$

162   Equation 20 represents the ideal wetting in the absence of gravity. In a real process without gravity,
163   part of the available surface energy will be lost in the form of entropy during wetting and A_k will be
164   slightly smaller than A_o. This fact will ensure that the wetting continues from d' to κ and not go back to the
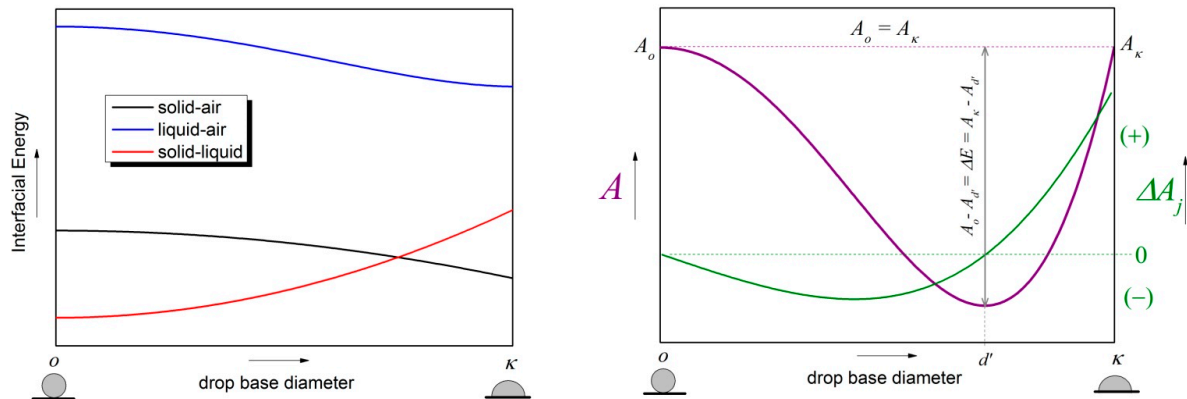165   initial configuration o.

166

167   **Figure 2.** Schematic representation of the energetic changes of a system while a drop spontaneously wets a
168   solid surface without the effect of gravity.

169   Continuing with the ideal model of spontaneous wetting, from Equation 20:

$$\Delta A_{o \to \kappa} = \gamma_L \Omega_L^\kappa + \gamma_{SL} \Omega_{SL}^\kappa + \gamma_S \left(\Omega_S^o - \Omega_{SL}^\kappa \right) - \gamma_L \Omega_L^o - \gamma_S \Omega_S^o = 0 \tag{22}$$

170   That results in:

$$\gamma_L \left(\Omega_L^\kappa - \Omega_L^o \right) + \left(\gamma_{SL} - \gamma_S \right) \Omega_{SL}^\kappa = 0 \tag{23}$$

171   A parameter κ can be now defined as:

$$\kappa = \frac{\Omega_L^o - \Omega_L^\kappa}{\Omega_{SL}^\kappa} \tag{24}$$

172   κ is a dimensionless parameter that characterizes a liquid drop at equilibrium, resting on a flat
173   surface without the effect of gravity. Under the condition of weightlessness, this parameter is, in principle,
174   independent of the size of the drop and not equivalent to the cosine of the contact angle of Young's
175   model:

$$\gamma_{SL} - \gamma_S = \kappa \gamma_L \tag{25}$$

176   In the Young's model, $\cos\theta_Y$ represents the bi-dimensional fraction of the liquid surface tension acting
177   horizontally on the triple contact point solid-liquid-gas. By contrast, for SDACC, κ represents the ratio of
178   the liquid-gas interface area-decrease and the solid-liquid interface area created by wetting (Eq. 24). In
179   other words, for a defined solid surface, κ represents the balance between the surface tension of the liquid
180   and the interfacial solid-liquid energy. While $\cos\theta_Y$ applies only to the boundary line of the bi-dimensional
181   drop profile, κ applies to all the interfaces of the three-dimensional system.
182   Let's consider now, as initial condition –configuration G-, a drop resting in equilibrium on a solid
183   and flat surface under the effects of the terrestrial gravitational field ($a_1=-g_E$, $g_E=9,81m/s^2$), see Figure 3a.

184   Suppose that the system is inside a closed capsule that is submitted to the free fall under controlled
185   conditions.
186   If a_2 is the acceleration of the uniformly accelerated motion of the capsule downwards, in the case of
187   the free fall, its value is obviously $-g_E$. This will switch off the effects of the gravitational field inside the
188   capsule that contains the surface and the drop. The resulting acceleration of this system will be given by:
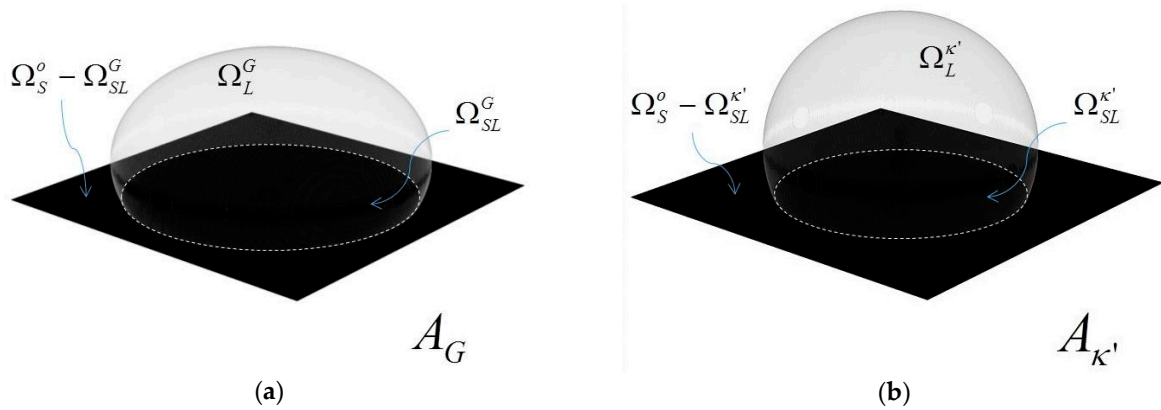
$$a^* = -a_2 + a_1 \qquad (26)$$

(**a**)   (**b**)

189   **Figure 3.** By the free fall, the energy that the terrestrial gravitational field is producing on the droplet (**a**) is
190   released, letting the droplet reach a new equilibrium only governed by the interfacial energies (**b**), which
191   shape is a spherical dome.

192   So, in the case of free fall, $a^* = 0$, that corresponds to an inertial system inside the capsule. To reach
193   this condition, the energy with which the terrestrial gravitational field is flattening the drop must be
194   released, letting the drop reach a new equilibrium state (Figure 3b) only governed by the interfacial
195   energies –the configuration κ'-. Macroscopically, it will result in the receding of the drop by the decrease
196   of the interfacial area and its "deformation" to a perfect sphere due to the increase of its height. The
197   acceleration that modifies the drop shape during the very short time of the mentioned energy release
198   process is given by a_f:

$$a_f = -a_2 \qquad (27)$$

199   During the energy release process, the receding of the drop will result in contact angle hysteresis. The
200   multiplicity of apparent contact angles, which is an essential feature of contact angle hysteresis, is
201   associated with the multiplicity of equilibrium states that a drop may assume on a rough or
202   heterogeneous surface [39]. One apparent contact angle is associated with the stable equilibrium state (the
203   global minimum in the free energy of the system). The others are linked to metastable equilibrium states
204   (local minima in the free energy). The transition between metastable states, toward the stable equilibrium
205   state, depends on the energy available to the drop for overcoming the energy barriers which inherently
206   exist between the metastable states [39].
207   By definition, the phenomenon of hysteresis is observed when a parameter of the system, such as the
208   volume of a drop placed on a solid, is varied back and forth, or when an external force is making the drop
209   move in one direction (ie., by the tilting table experiment). In SDACC, the release of gravitational energy
210   makes the contour of the drop recede on the surface and experience hysteresis. For this reason, this
211   microgravity model is, in principle, oriented to characterize chemically homogeneous and smooth
212   surfaces.
213   According to Grundke [40], while the advancing contact angle is expected to represent the property
214   of the predominant material of the surface, the receding contact angle is only a manifestation of the

215 impurities of that solid surface. It has been shown [39], that the contact angles assumed by the drop
216 during advancing or receding is oscillatory. These oscillations may explain the macroscopic stick-slip
217 behavior which is observed during contact angle hysteresis measurements. SDACC does not take into
218 account the contact angle values, because they only provide information about balance on the drop line
219 contour. However, the hysteresis effect occurs during the drop recedes, and it can modify the increase-
220 decrease of the interfacial areas during de-wetting. In any case, SDACC evaluates the shape of the droplet
221 in the stable equilibrium state (κ'), when the transition between metastable states (hysteresis) is already
222 concluded. In this configuration, without the effects of gravity, the drop shape is a spherical dome.
223   Going back to the case of the sessile drop in the free fall, the acceleration experienced by the drop for
224 the short time of the energy release is $a_f = +g_E$, i.e., a short duration force acting upwards. The mechanical
225 work that the drop must make to modify its shape and release surface energy is given by W_M.

$$-W_M = \Delta A = A_{\kappa'} - A_G \tag{28}$$

226   From the standpoint of the drop, this work can also be divided into two components: the work W_P
227 necessary to move up its center of mass and the work W_S necessary to radially move the contour line
228 solid-liquid-gas during a short de-wetting process (Figure 4).

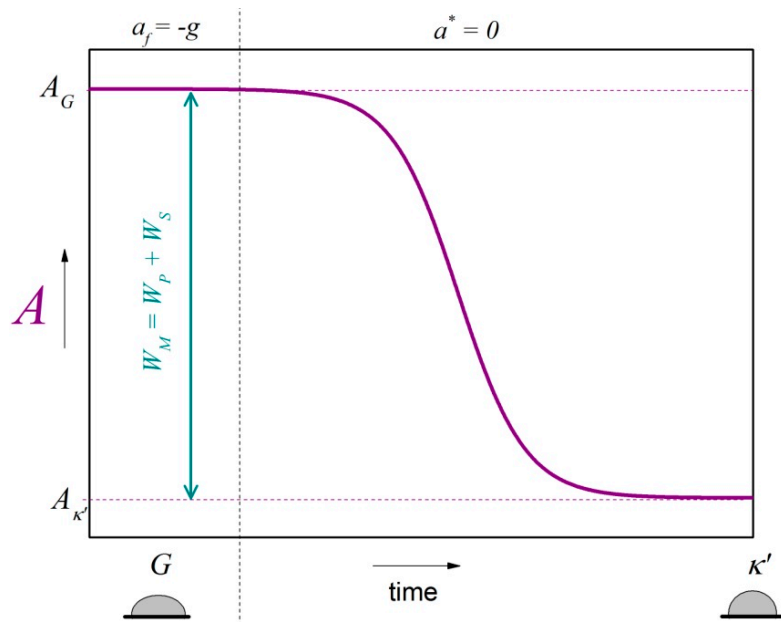$$W_M = W_P + W_S \tag{29}$$

229

230   **Figure 4.** The free-fall makes the system release the energy with which the gravitational field was
231   deforming the drop. The Helmholtz energy of the drop in the form of interfacial energies is released,
232   resulting in a drop with a spherical dome shape, the configuration κ'.

233   The change in the potential energy of the droplet can be calculated by measuring the change in the
234 position of all the liquid particles, by considering for a moment the liquid as a particle system. If a particle
235 system is changing from the state *1* to the state *2*, their potential energies under a force field that produces
236 the acceleration a_f, can be described by:

8

$$e_{p1} = \sum_{i}^{n} m_i\, a_f\, z_{1i} \tag{30}$$

237

$$e_{p2} = \sum_{i}^{n} m_i\, a_f\, z_{2i} \tag{31}$$

238 Where m_i is the mass of each particle and n the total number of particles. The change in potential
239 energy from state *1* to state *2* is given by:

$$W_p = a_f \left(\sum_{i}^{n} m_i\, z_{2i} - \sum_{i}^{n} m_i\, z_{1i} \right) \tag{32}$$

240 The center of mass of a particle system is defined by:

$$z_c = \frac{\sum_{i}^{n} m_i\, z_i}{m} \tag{33}$$

241 Then, the Equation 32 for the potential energy necessary to move all the liquid particles from the
242 state G to κ', can be written as:

$$W_p = m a_f \left(z_{c\kappa'} - z_{cG} \right) = \rho V a_f \left(z_{c\kappa'} - z_{cG} \right) \tag{34}$$

243 Where ρ is the density of the liquid and V is the drop volume.
244 The second component of the work that the drop must make, the energy necessary to produce the
245 receding wetting during its deformation from the state G to κ', can be calculated by the integration of all
246 the differentials of energy needed to move the contour line on the surface in the radial direction (Figure 5):
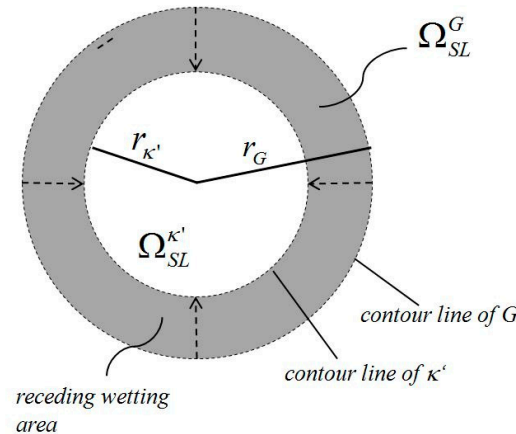

247 **Figure 5.** The drop profile observed from above: the release of the force field leads to dewetting. A receding
248 work decreases the interfacial area from Ω^G_{SL} to Ω^κ_{SL}.

$$\int_{G}^{\kappa'} dW_s = \int_{G}^{\kappa'} \tau\, l\, dr \tag{35}$$

249   Where τ is tension necessary for the drop to move the contour line on the surface, l is the length of the
250   contour line and r the radius of the wetting area Ω_{SL}. These considerations result in:

$$W_s = 2\pi\tau \int_G^{\kappa'} r\, dr \tag{36}$$

251   Which, in turn, results in:

$$W_s = \tau\pi\left(r_{\kappa'}^2 - r_G^2\right) = \tau\left(\Omega_{SL}^{\kappa'} - \Omega_{SL}^G\right) \tag{37}$$

252   At the equilibrium, the work made by the drop –the energy released- will result in energy changes on
253   the system surfaces. Equations (28), (29), (34) and (37) result in:
254

$$-\rho V a_f\left(z_{c\kappa'} - z_{cG}\right) - \tau\left(\Omega_{SL}^{\kappa'} - \Omega_{SL}^G\right) = \gamma_L\left(\Omega_L^{\kappa'} - \Omega_L^G\right) + \gamma_{SL}\left(\Omega_{SL}^{\kappa'} - \Omega_{SL}^G\right) + \gamma_S\left(\Omega_S^o - \Omega_{SL}^{\kappa'} - \Omega_S^o + \Omega_{SL}^G\right) \tag{38}$$

255   Making the corresponding arrangements:

$$\left(\gamma_{SL} - \gamma_S + \tau\right)\left(\Omega_{SL}^{\kappa'} - \Omega_{SL}^G\right) = -\gamma_L\left(\Omega_L^{\kappa'} - \Omega_L^G\right) - \rho V a_f\left(z_{c\kappa'} - z_{cG}\right) \tag{39}$$

256   In the case of a free fall, both terms at the left side of Eq. 38 must give negative values because the
257   drop must release energy to deform its shape, i.e. it must do work. By the first term, the acceleration and
258   the difference of center of mass are both positive, resulting in a negative term due to the minus sign ahead
259   of it. The second term is also negative, because the minus sign, the negative value of the areas difference –
260   receding wetting- and the value of τ, which is negative due to the following reason: during the dewetting
261   of the drop contour, the tension τ is the force that the liquid must overcome to recede on the solid surface,
262   i.e., to "create" solid surface. This surface tension is the opposite of the previously defined surface energy
263   of the solid γ_S:

$$\tau = -\gamma_S \tag{40}$$

264   Under this consideration, the Equation 39 can be written as:

$$\gamma_{SL} - 2\gamma_S = \frac{-\rho V a_f\left(z_{c\kappa'} - z_{cG}\right) - \gamma_L\left(\Omega_L^{\kappa'} - \Omega_L^G\right)}{\Omega_{SL}^{\kappa'} - \Omega_{SL}^G}, \quad a_f = +g_E, \; \textit{free fall} \tag{41}$$

265   Summarizing, in the case of the free fall, $a_2 = -g_E$ (capsule is falling) and $a_1 = -g_E$ (terrestrial
266   acceleration acting on the droplet in rest). So, the net acceleration that deforms the droplet for a very short
267   time during the free fall is $a_f = +g_E$, i.e. a short duration deformation force from bottom to up. However,
268   once the drop reaches the equilibrium inside the capsule, it will be found within a system with zero
269   acceleration, ie. $a^* = 0$ (weightless). In consequence, at the end of the experiment (configuration κ'), the
270   drop will be resting in stable equilibrium inside an inertial system.
271   The configuration κ, as mentioned before, is reached ideally after the end of a very fast wetting
272   process that started spontaneously with the configuration o without the effect of the gravity. In the
273   microgravity method, however, the configuration κ is quantified in a special way: the capsule with a drop
274   in the configuration G, i.e., resting under the effects of the terrestrial gravity ($a_1 = -g_E$, $g_E = 9.81 m/s^2$) is moved
275   downward with $a_2 = -g_E$, (free fall). This results, as seen above, in a sudden upward acceleration $a_f = +g_E$
276   that deforms the drop for some moment (milliseconds in practice) until it reaches the weightlessness state
277   ($a^* = 0$) inside the capsule (inertial system), the so-called configuration κ'. The present model proposes that
278   the configuration κ' resulting from this forced de-wetting process is the same as the configuration κ, or at
279   least quite similar.
280   By analyzing the images provided by the high-speed camera using Axisymmetric Drop Shape
281   Analysis (ADSA) or ellipse matching, it is possible to find the frames where the droplet is resting free of

282   vibrations with a perfectly spherical shape (the ellipse matching is highly recommended). These images
283   correspond to the configuration $\kappa=\kappa'$ of the model. The values of the interfacial areas $\Omega^o{}_L$, $\Omega^\kappa{}_L$, and $\Omega^\kappa{}_{SL}$
284   can be obtained by the drop volume, the matching method and the formulas that are presented below, to
285   obtain the value of the parameter κ, using the Eq. 24.
286   It is important to mention, that for the application of any drop-shape analysis method it is essential
287   that the drop is completely axisymmetric. In other words, the wetting has to be completely isotropic. In
288   the case of topographic anisotropy, it should be only nanometric and not affect wetting. Otherwise, it
289   would be necessary to analyze the geometry of the drop in three dimensions. Some manufacturers of drop
290   shape analyzers, like Krüss GmbH (Germany), have already begun to develop top-view distance optical
291   methods for capturing the curvature of the drop to measure contact angles on curved solid surfaces and in
292   depressions which are not easily accessible to the classical drop shape analysis. The combination of this
293   technology with SDACC could make possible its application for non-axisymmetric drops on anisotropic
294   surfaces.
295   The values of the interfacial areas $\Omega^G{}_L$, and $\Omega^G{}_{SL}$ can be obtained from the first frames some
296   milliseconds before starting the free fall. This instant corresponds to the drop resting in equilibrium under
297   the effects of gravity, the configuration G. The drop centers of mass z_{CG} and $z_{C\kappa'}$ can be calculated from the
298   initial images and the images of configuration $\kappa=\kappa'$, by applying the Equation 51 given below. The exact
299   value of the acceleration a_f, can be obtained from the accelerometer of the instrument (see the
300   Experimental Section).
301   The values of γ_S and γ_{SL} can be obtained by solving the system given by the equations 25 and 41. For
302   the application of the microgravity method, it is only necessary to know the value of the surface tension of
303   the liquid, its density, and the drop volume.
304   The precision of SDACC is highly dependent on the precision of the interfacial areas measurement.
305   During the energy release of the drop, it could move some micrometers on the camera view-axis. As a
306   consequence, the scale of the frames could change a little bit during the process. For this reason, the drop
307   shape matching algorithms must be carefully scaled to evaluate the drop shapes of the configurations $\kappa=\kappa'$
308   and G with the same drop volume.
309   The artificial accelerations produced inside the capsule result in drop deformations given by a_f. Two
310   cases of spheroidal caps [41-44] must be differentiated to calculate the values of the solid-liquid Ω_{SL} and
311   the liquid-air Ω_L interfacial areas: $a^*=0$ and $a^*<0$.

312   *Case I: sphere cap [42], $a^* = 0$*

313   The radius of the solid-liquid interface is given by:

$$R = \sqrt{h\left(2\,b - h\right)} \tag{42}$$

314   Where h is he height and b the radius of the partial sphere, according to Figure 6a.
315   The volume of the partial sphere is given by:

$$V = \frac{\pi}{6}\,h\left(3\,R^2 + h^2\right) \tag{43}$$

316   The surface area –the interfacial area liquid-gas- is given by:

$$\Omega_L = \pi\left(R^2 + h^2\right) = 2\,\pi\,b\,h \tag{44}$$

317   And the interfacial area solid-liquid is given by:

$$\Omega_{SL} = \pi\,R^2 \tag{45}$$

318

$$a^* = 0 \qquad\qquad\qquad a^* < 0$$

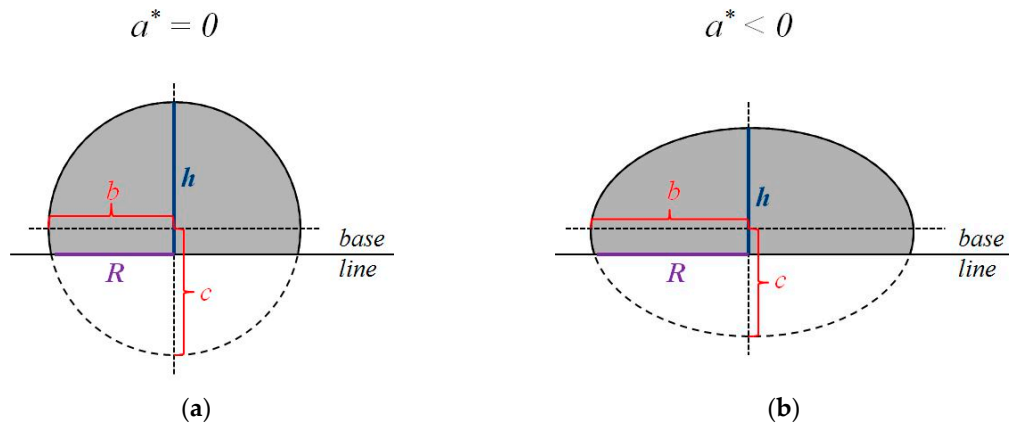(a)   (b)

319
320

Figure 6. Profiles of the two possible spheroids of the droplet shape during the free fall: (a) sphere and (b) oblate. The 2D- profiles of the spheroid caps are in gray.

321   *Case II: oblate cap [41], $a^* < 0$*

322   The radius of the solid-liquid interface is given by:

$$R = b\sqrt{1 - \left(1 - \frac{h}{c}\right)^2} \tag{46}$$

323   The volume of the oblate is given by:

$$V = \frac{\pi}{3}b^2 c \left(\frac{h}{c}\right)^2 \left(3 - \frac{h}{c}\right) \tag{47}$$

324   where b, c and h are the magnitudes according to Figure 6b.
325   The interfacial area solid-liquid is given by:

$$\Omega_{SL} = \pi b^2 \left[1 - \left(1 - \frac{h}{c}\right)^2\right] \tag{48}$$

326   And the surface area –the interfacial area liquid-gas- is given by:

$$\Omega_L = \pi b c \left\{ \frac{b}{c} - \left(1 - \frac{h}{c}\right)\left[1 + \varepsilon^2\left(1 - \frac{h}{c}\right)^2\right]^{1/2} + \frac{1}{\varepsilon}\left(ar\sinh(\varepsilon) - ar\sinh\left[\varepsilon\left(1 - \frac{h}{c}\right)\right]\right)\right\} \tag{49}$$

327   where:

$$\varepsilon^2 = \frac{b^2}{c^2} - 1 \geq 0 \tag{50}$$

328   In both cases: sphere and oblate cap, the center of mass of the cap can be calculated using [41]:

$$z_c = \frac{h}{4}\frac{4 - \dfrac{h}{c}}{3 - \dfrac{h}{c}} \tag{51}$$

12

329   **3. Experimental Section**

330   The instrument [35] consists of a vertical tower three meters tall with all the necessary elements to
331   control the accelerated movement of a capsule containing the solid-liquid-gas system during a time span
332   from 600 to 750 milliseconds. The tower (Figure 7) was originally constructed to allow the motion of the
333   capsule under different acceleration values upwards and downwards. However, the present study is
334   focused on the free-fall mode, i.e. the instrument as a microgravity tower.

335   The components of the instrument are: the upper ignition device (1), the lower ignition device (2), the
336   displacement tower (3), the acceleration device (4), the braking or damping mechanism (5) the liquid
337   dosing device (6) and the capsule with the sample (7). Further, the instrument is connected to a computer
338   with the software necessary to control the devices and evaluate the data.

339   The upper ignition device (1), as well as the lower ignition device (2), are electromagnetic
340   mechanisms designed to release the anchored capsule so it can move freely by the action of the
341   acceleration device. They are designed to minimize the vibrations during the ignition. The displacement
342   tower (3) is designed to guide the capsule in the vertical direction without vibration and minimizing the
343   effects of friction. The acceleration device (4) actuates the capsule in values of constant acceleration using
344   the linear increase of the speed starting from the rest (zero velocity). This device is capable of moving the
345   capsule both upwards and downwards. In the case of the downward drive with the acceleration of $-g_E$
346   (Earth gravitational field), it is possible to let the capsule simply fall free with the help of the guide
347   elements of the shift tower. The acceleration device may be a servo motor capable of producing constant
348   accelerations upwards or downwards of any value or a mechanical device which, based on a combination
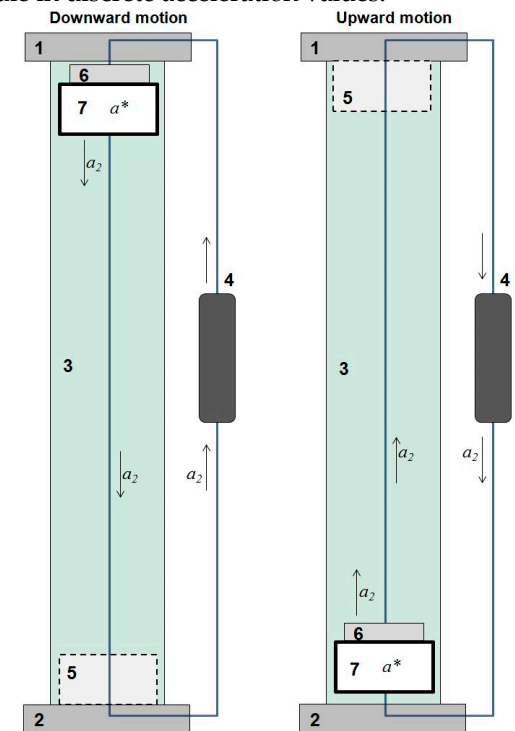349   of pulleys, moves the capsule in discrete acceleration values.

350   **Figure 7.** The measure capsule (7) can be moved upwards or downwards.

351   The damping mechanism (5) consists of a mechanical, pneumatic or hydraulic arrangement capable
352   of decreasing the velocity without increasing the acceleration above $20g_E$ to not damage the devices inside
353   the measuring capsule. Depending on the orientation of the movement, it can be installed on the top or
354   bottom of the tower.

13

355   The liquid dosing device (6) must be able to dose small droplets from 5µL to 100µL on the sample
356 surface inside the capsule. It can consist of an arrangement of a micro-pump and dosing cannula or a
357 mechanic or electronic micropipette. In the first case, it could be attached and moved together with the
358 microcapsule. In the case of a micropipette, it could be triggered independently of the tower structure.
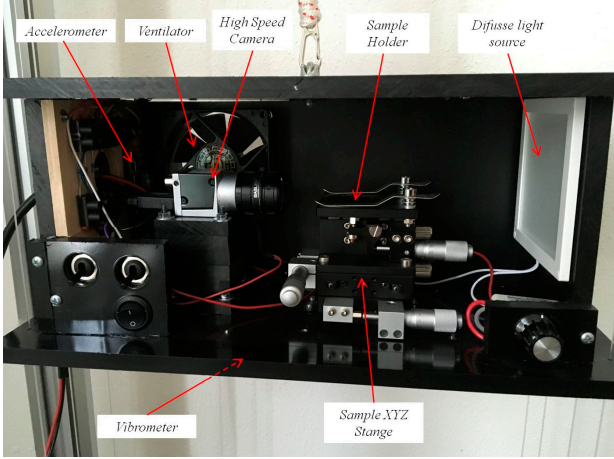

359   **Figure 8.** Measuring capsule with the high-speed camera, XYZ-stage, light diffusion source, accelerometer
360   and vibrometer and cooling system.

361   The measuring capsule consists of a high-speed camera (100 – 1000 frames per second, fps), a sample
362 stage (XYZ), a diffuse light source, an accelerometer, a vibrometer and a refrigeration unit (ventilator)
363 (Figure 8). This device can obtain images or video of the drop during its motion with good resolution at
364 higher fps values. The diffuse light must provide a good illumination and allows a good contrast to obtain
365 sharp drop contours. The stage will be used to put the sample in the optimal position for the experiment.
366 The accelerometer and the vibrometer measure the values of the acceleration (Z-Axis) inside the capsule
367 and the values of the accelerations in X- and Y-axis to evaluate the vibration during the experiment,
368 respectively. The ventilator is used to cool the high-speed camera between the measurements.
369   The first published results of SDACC [35] were realized using polypropylene (PP) and
370 polytetrafluoroethylene (PTFE) surfaces. For the present study, new tests were realized using seven
371 smooth polymer surfaces -including new PP and PTFE-, which details and relevant topographic
372 parameters are listed in Table 1.

373   **Table 1.** Polymer surfaces and roughness

Polymer material	Description	Sa(1), nm	Sdr(2), %	Iso(3), %
Polypropylene, **PP**	5 mm thickness, translucent with protection film (al-intech, Germany)	28	0.236	66,13
Polyethylene, **PE**	High density (HD) PE, 5 mm thickness, black (al-intech, Germany)	128	0.606	70,10
Polytetrafluoroethylene, **PTFE**	Teflon, 2 mm thickness, white, (Alt Industriebedarf, Germany)	301	6.070	23,13
Poletyhelene terephthalate, **PET**	Polyester PET-G, 1 mm thickness, transparent with protection film (Hbholzmaus Kunstoffe, Germany)	3	0.026	65,07
Polystyrene, **PS**	2 mm thickness, black, (az-reptec, Germany)	698	3.097	68,47
Polymethyl methacrylate, **PMMA**	Acrylglas, 2 mm thickness, transparent with protection film (GeerGroup UG, Germany)	2	0.019	62,10

14

Polyvinylchloride, **PVC**	2 mm thickness, white with protection film (kunstoff-city, Germany)	230	2.667	6,97

374   [1] Surface arithmetic mean roughness; [2] Developed surface area ratio; [3] Texture Isotropy

375   The topographic characterization was carried out using high-resolution ScanDisk Confocal
376   Microscopy (SDCM). The SDCM device was a µsurf explorer (Nanofocus AG, Germany). An objective
377   with the magnification 100X was used, which provides a measure length of 160 µm and lateral and
378   vertical resolutions of 0.3 µm and 2 nm respectively. Three measurements were carried out on different
379   positions of the samples. The topographic parameters arithmetic mean roughness *Sa* and developed
380   surface area ratio *Sdr* (Table 1) show that the roughness of the materials is small enough to consider the
381   surfaces smooth for the experiments. The texture isotropy, calculated using the MountainsMap®
382   Premium Software (Digital Surf sarl, France) show that the PP, PE, PET, PS and PMMA surfaces are
383   isotropic enough to consider that the drop will form axisymmetric shapes. The morphology of these
384   surfaces was only slightly affected by negligible scratches due to manipulation. In case of PTFE and PVC,
385   however, the anisotropy is structural. However, the nanometric- scale roughness of these surfaces, 301
386   and 230 nanometers respectively, should not significantly affect the axisymmetry of the 15 µL water
387   droplets (approx. 4-5 mm of base diameter) that will be deposited on them.
388   The materials were cut into 5 x 5 cm^2 samples and submitted to the tests with the microgravity lab
389   tower.

4. Results

391   The calibration of the apparatus was realized according to [35], using a *R-DAS Tiny rocket*
392   *accelerometer V4.0* (AED Electronics, USA) to measure the microgravity and a USB *Vibration Logger DL-*
393   *131G* (Voltcraft, Germany) to determine and control the lateral vibrations during the gravitation release.
394   After a couple of mechanical improvements on the original prototype to control the vibrations during the
395   ignition and decrease the friction during the fall, the resulting reduced gravity [42] inside the capsule was
396   *a* = +0.0018 g$_E$*
397   The effect of gravity on the macroscopic advancing contact angle was studied in 2005 by Ababneh et
398   al. [21] using experiments in a specially modified FALCON 20 business jet (NRC Flight Research
399   Laboratory, Canada) that flies a parabolic arc to produce short periods of reduced net acceleration force.
400   The authors reported important irreproducibility of the contact angle due to the airplane vibration. The
401   use of drop towers also presents the difficulty of the vibration produced during the ignition, i.e. during
402   the release of the capsule to the free fall. Recent experiments realized in 2012 by Diana et al. [22] using the
403   Drop Tower Facility of the Queensland University of Technology (Queensland, Australia) and Zhu et al.
404   [23] using the Drop Tower of Beijing (National Microgravity Laboratory, Beijing, China) showed that the
405   simple wire cutting release mechanism that initiates the drop of the experimental rack induces vibrations
406   on the drop. According to [22], the sudden variation of the gravity force induces oscillations in the sessile
407   drop. Indeed, at the beginning of the test, the energy stored in the thin wire that was holding the
408   experimental package and drag shield was released resulting in vibrations in the sessile droplet. The
409   vibrations using the microgravity tower prototype for the present study are important during the first 250
410   milliseconds of the experiment. From 450 milliseconds onwards they are negligible.
411   The experiments using the Drop Tower of Beijing [23] report a stabilization time from 0.8 to 1.2
412   seconds in the case of sessile drops, while by the experiments using the Drop Tower Facility of
413   Queensland [22], the vibration time for sessile drops to reach equilibrium is less than 0.5 seconds. These
414   authors carefully observed the transition from formal to reduced gravity using a 30 fps camera.
415   It is important to mention that the study of Diana et al. [22] was oriented to present an initial work to
416   develop a database of contact angles of sessile droplets in reduced gravity and to study the dimensional
417   variations due to the increase of the drop size regarding Bond number. The study of Zhu et al. [23] was
418   oriented to investigate the influence of Bond number on behaviors of liquid drops deposited onto solid

419   substrates and to probe the effectiveness of a simulation model. None of these studies was oriented to
420   study or measure the surface energies of the substrates.
421   Small drop towers only exist for educational and demonstrative purposes [45-46]. However, apart
422   from the study of Calvimontes [35], which is the basis for the present work, there are currently no reports
423   about the study of wetting and measurement of surface energies using the release of gravitation.
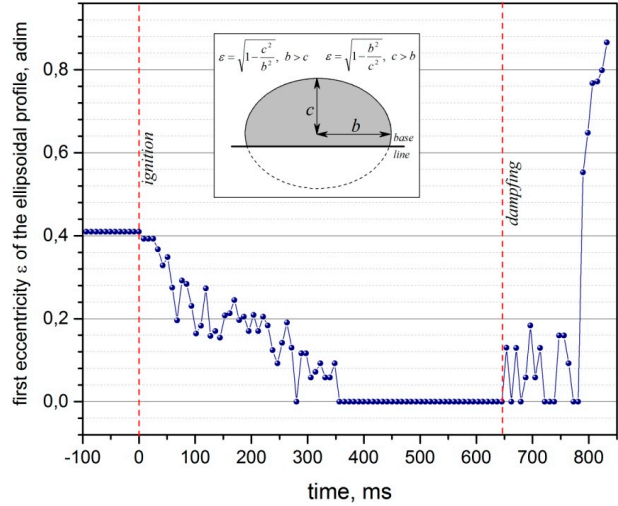
424   **Figure 9.** Vibration release of water drops on a PP surface regarding drop shape eccentricity. 76 frames
425   were analyzed from the 480 available (750 fps video recording) [35].

426   To quantify the stabilization time of the droplets during the experiment, the first eccentricity, ε, was
427   used in [35]. This parameter was defined in the equation 50 for the oblate ($b>c$) case. A perfect sphere ($b =$
428   c) with $\varepsilon = 0$ in the microgravity region confirms that the effects of vibration were released. According to
429   Figure 9, the eccentricity for doubled distilled water droplets of 20 μL on the PP surface shows that the
430   vibration is completely released after 350 milliseconds of the ignition.
431   The calculation of the interfacial areas is possible using the equations 44 and 45. The values obtained
432   for the parameter κ' on all the seven surfaces are listed in Table 2. Ten measurements corresponding to ten
433   different drops were made for 15 μL bi-distilled water droplets on each surface at 22±1 °C of temperature
434   and 60±2 % of relative humidity. According to [35], the optimal volume for the experiment using water is
435   between 10 and 20 μL because in this interval both, the surface tension and the gravitation, are governed
436   the wetting and the drop shape. According to [22], there are two forces that principally produce the
437   droplet shape: the surface tension of the liquid, which tends to minimize the area of the surface
438   (producing the spherical shape) and the gravitational force which tends to flatten the droplet.
439   Before initiating the free fall, the interfacial areas at the *G*-configuration, i.e. the sessile droplet under
440   the effects of the gravity, were measured using the droplet images. The droplet mass centers in the *G* and
441   κ' configurations were also measured for each experiment.
442   The interfacial energies were calculated by solving the system given by the equations 25 and 41 for
443   each experiment, i.e., for each pair of images corresponding to the *G* and κ' configurations. The results are
444   presented in Table 2.

445   **Table 2.** Results of the surface characterization

Polymer	κ'		γ_S, mJ/m²		γ_{SL}, mJ/m²	
Polypropylene, **PP**	0.5287	± 0.0058	30.8708	± 0.4070	69.3591	± 0.2354
Polyethelyne, **PE**	0.4030	± 0.0127	34.0385	± 0.5512	63.3805	± 0.7212

Polytetrafluoroethylene, **PTFE**	0.6199	± 0.0037	20.1871	± 0.5006	65.3167	± 0.5071
Poletyhelene terephthalate, **PET**	0.3564	± 0.0123	41.3845	± 0.3405	67.3328	± 0.9448
Polystyrene, **PS**	0.3376	± 0.0372	43.4610	± 0.7066	68.0411	± 2.5544
Polymethyl methacrylate, **PMMA**	0.1528	± 0.0192	49.2423	± 0.6394	60.3631	± 0.9917
Polyvinylchloride, **PVC**	0.3764	± 0.0073	34.5522	± 0.4563	61.9534	± 0.4893

446   During the free fall, the water droplet experienced receding wetting during approximately 450
447   milliseconds in case of the PP surface [35]. During this period, the system went through multiple transient
448   and metastable states that can be observed by the contact angle hysteresis in Figure 10. In this example,
449   the contact angles decrease from 93.8° to 92° due to the release of gravity. The oscillations due to the
450   energy barriers of the surface combined by the mechanical micro vibrations due to the electromagnetic
451   release of the capsule lead the droplet to the equilibrium (κ') through multiple metastable states.
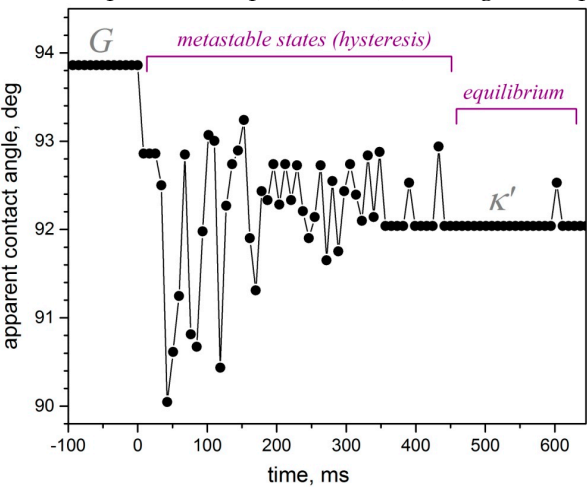

452   **Figure 10.** Contact angle hysteresis of a 20μL water droplet on a PP surface [35]. The transition from stable
453   state G, followed by metastable states (energy release) toward the stable equilibrium state of the
454   configuration κ'.

455   To compare the microgravity method with the Owens-Wendt [28] and Wu [30] methods,
456   measurements with a Mobile Surface Analyzer –MSA (Krüss GmbH, Germany) were realized using
457   doubled distilled water and diiodomethane (Sigma-Aldrich). For each of the seven surfaces, ten drops of
458   1μL were used. The results are presented in Figure 11.
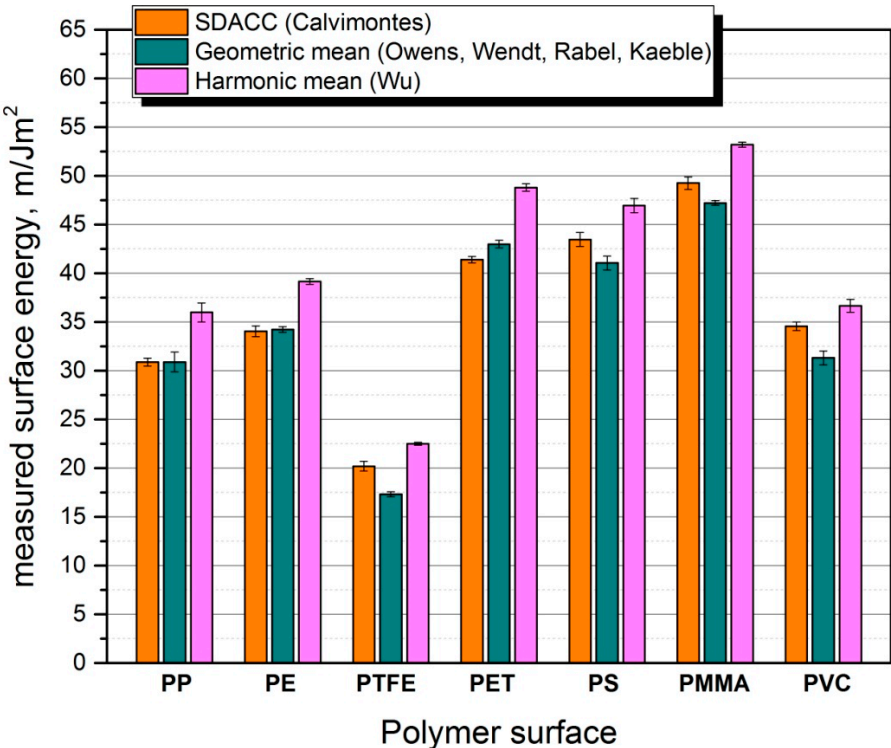
17

Figure 11. Comparison between the calculated values of γs for the seven polymer surfaces obtained by the methods Owens et al., Wu, and SDACC.

5. Discussion

According to the results, the SDACC correlates well with the results obtained by the method of Owens et al. [28] for Polypropylene (PP), Polyethylene (PE) and Polyethylene terephthalate (PET). The values obtained for the surfaces of Polytetrafluoroethylene (PTFE), Polystyrene (PS), Polymethyl methacrylate (PMMA) and Polyvinylchloride (PVC) are intermediate between the values obtained by the methods of Owens et al. and Wu. In all the cases, the values obtained by Wu tend to be considerable higher.

As mentioned above, recent experimental evidence using microgravity by parabolic arc flights [21] and microgravity drop towers [22-23] have demonstrated that the effect of gravity on the contact angle is relevant even at very small drop volumes such as 5 μL. According to Allen [24], who studied the wetting of very small drops with small contact angles, a drop is small enough to neglect gravitational influences only if its volume is less than 1 μL. For the present study, small droplets of only 1μL volume were used while applying the Owens et al. and Wu methods. However, the effects of the gravity are still significant on these droplets. To probe this, the eccentricity values of very small droplets on a PP and PTFE surfaces were measured using the Mobile Surface Analyzer –MSA (Krüss GmbH, Germany) instrument. The results can be seen in Figure 12. According to this, water droplets of only 1μL are still deformed by the gravitation: on PP surfaces, the eccentricity of the water droplet is 0.2179, while on PTFE surfaces is 0.1466.
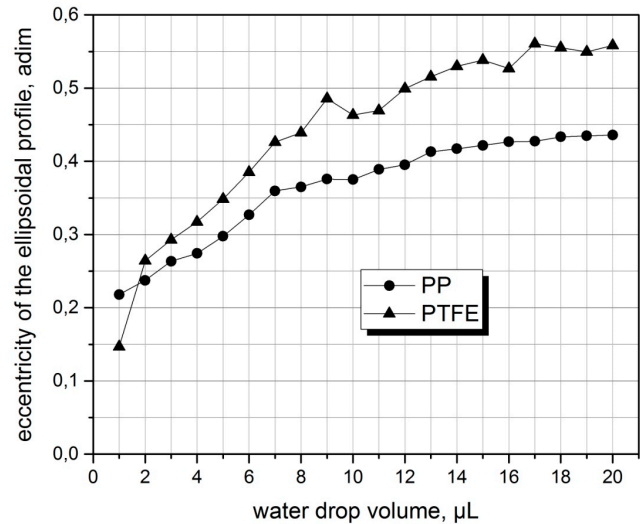
479   **Figure 12.** The eccentricity of different water droplets volumes on PP and PTFE surfaces. The drops are
480   deformed by gravity even when they are very small.

481   The deforming effect of the gravity on the droplet is not the only problem for determining the
482   interfacial energies using the typical contact angle methods like Owens et al. and Wu. The use of small
483   droplets leads additionally to the increase of the effects of the roughness on the contour line. Even smooth
484   surfaces have micro- and nanometric inhomogeneities that could affect the solid-liquid-gas contour line of
485   the droplet. And this is very relevant when the method used is based only on the geometry of the
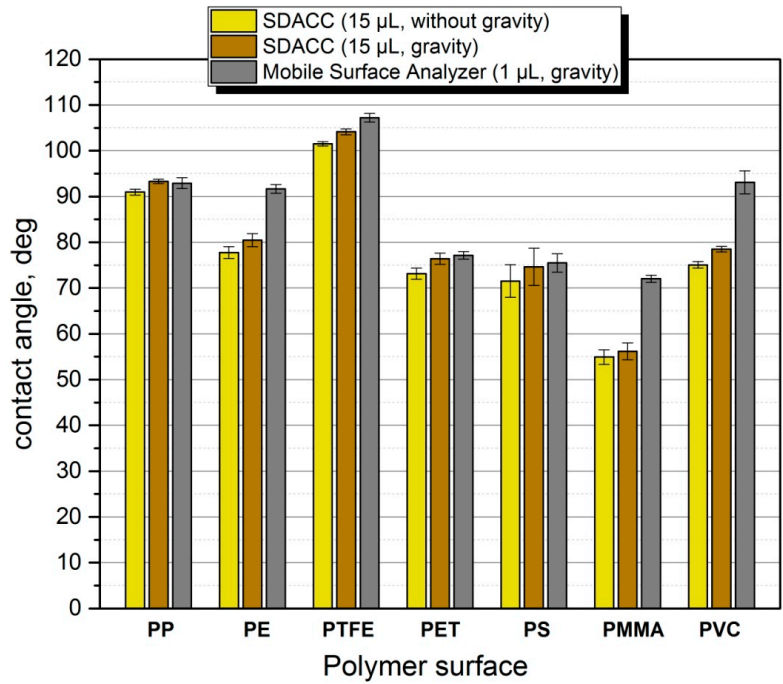486   boundary solid-liquid-gas.

487   **Figure 13.** Comparison of the measured contact angles of a 15 μL water droplet with and without the effect
488   of gravity, and 1μL droplet under the effect of gravity.

19

489   Figure 13 compares the measured contact angles before and after the gravitation release using 15 μL
490 drops, with the contact angles measured by the MSA instrument using 1μL drops under the effect of
491 gravity. According to this data, the measured contact angles in the microgravity are always lower than the
492 measured under the gravitational effects. This is to be expected for contact angles greater than 90 degrees
493 –PP and PTFE-, according to [21]. However, when the contact angles in the microgravity are lower than 90
494 degrees it would be predictable, according to [21], that the gravitation decreases the contact angles slightly
495 by promoting wetting. However in all the studied cases -especially for PE, PMMA and PVC measured by
496 the MSA device (Krüss Germany) using 1 μL drop volume-, the contact angles are larger under the effects
497 of gravity.

498   There are, in principle, two explanations for this effect while comparing the droplets of 15 μL with
499 and without the effects of gravity. The first hypothesis is that the gravity release leads to receding wetting
500 due to the release of gravitation: in all the cases, larger or smaller contact angles, the effect of micro- and
501 nano-roughness of the surfaces by the stick-slip effect would also be modifying –decreasing- the contact
502 angles on the contour line of the droplet at equilibrium (configuration κ'). However, this small alteration
503 of the wetting due to the contact angle hysteresis would affect principally the boundary of the droplet and
504 would be negligible for the resulting value of the whole interfacial area solid-liquid. In any case, the
505 vibrations due to the gravitation release during the experiment could also help the droplets to recede and
506 overcome the energy barriers easily. The second hypothesis, that will be discussed in detail later, is related
507 with the singular hydrophibicity-hydrophilicity threshold of SDACC at the value $\kappa = 0$ ($\theta_Y = 42.88°$).

508   To explain the considerable larger contact angles of PE, PMMA and PVC under gravity while using 1
509 μL after a dosing process by advancing wetting (MSA instrument, see Figure 12), it is necessary to take a
510 look at the micro- and nanoroughness, that would be stopping wetting on the solid-liquid-gas contour
511 line -and consequently increasing the contact angles-, due to the small drop size (1 μL). The effect of
512 advancing and receding wetting is the main cause of inaccuracy when the surface energy characterization
513 is based on the measurement of apparent contact angles on the boundary line only –even if they are at
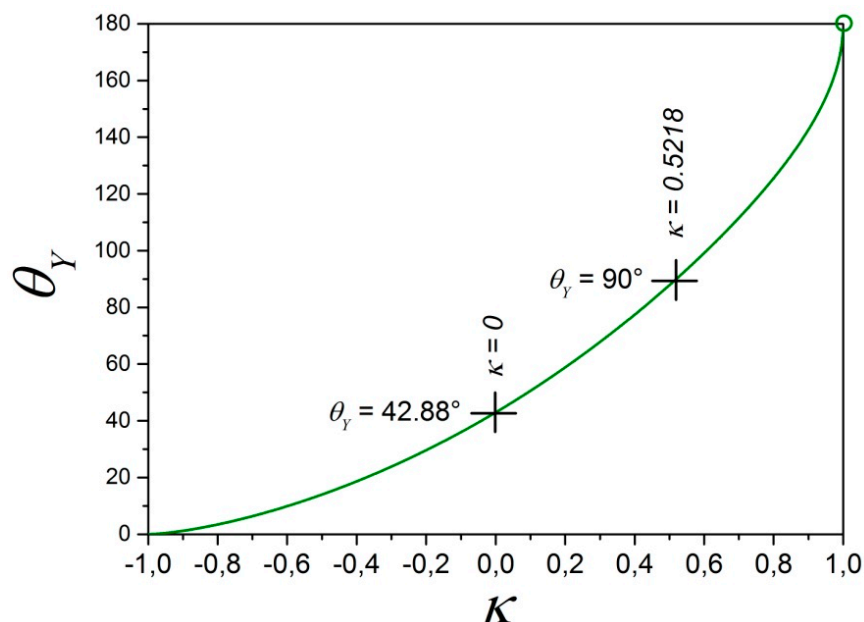514 stable equilibrium-, and not on the changes on the interfacial surfaces.

515 **Figure 14.** The relationship between Young's contact angle (equivalent to the contact angle without gravity,
516 θ_κ) and the parameter κ.

517   As mentioned above, in Young's model $cos\theta_Y$ represents the bi-dimensional fraction of the liquid
518   surface tension acting horizontally on the triple contact point solid-liquid-gas. By contrast, in SDACC, κ
519   represents the ratio of the liquid-gas interface decrease and the solid-gas interface created by wetting (Eq.
520   24). While $cos\theta_Y$ applies only to the boundary line of the bi-dimensional droplet profile, κ applies to all the
521   interfaces of the three-dimensional system.

522   A relationship between κ and θ_Y can be built by means of a mathematical simulation considering a
523   spherical drop of any liquid that virtually wets and spreads from θ_κ = 180° to θ_κ = 0° on any smooth
524   surface in absence of gravity. By the definition of Young's equation, $\theta_Y = \theta_\kappa$, because the Young's model
525   considers no effect of gravity. According to Figure 14, the relationship between θ_Y and κ is near to an
526   exponential with a κ-domain [-1; 1[. If $\theta_Y \rightarrow$ 180°, then $\kappa \rightarrow$ 1. But if θ_Y =180°, κ is not defined because it
527   results in a division by zero, according to Eq. 24, where, in this case, the interfacial area solid-liquid does
528   not exist anymore.   For the wetting models based on the Young's equation, the transition hydrophobic-
529   hydrophilic is given by definition at 90 degrees. By SDACC, θ_κ = 90° corresponds to κ = 0.5218 and,
530   apparently, does not represent any relevant point for the function $\theta_Y = f(\kappa)$, as can be seen in Figure 14. The
531   threshold between hydrophobicity and hydrophilicity at θ_Y = 90° is a characteristic result of the force
532   balance in the three-phase contact point of Young's model. Instead, by SDACC, the pole κ = 0 represents a
533   very interesting point: in this, according to Equation 24, the interface liquid-air of the sessile drop equals
534   the value of the liquid-air interfacial area of the original spherical drop before wetting. As mentioned
535   before, by the Young's equation (Eq. 1), if the surface energy (in mJ/m^2) of the solid equals the tensor (in
536   mN/m) of the solid-liquid contour, then the contact angle is 90 degrees ($cos\theta_Y$ = 0), while by SDACC, the
537   surface energy of the solid equals the energy of the solid liquid interface only if κ = 0. The contact angle, in
538   this case, is θ_κ = 42.88°. This value is the threshold hydrophobicity-hidrophilicity of the thermodynamic
539   model for SDACC.

540   Young's model considers an interfacial solid-liquid tensor on the contour line. Let's rename this
541   parameter σ_{LS} to differentiate from the interfacial energy γ_{SL} defined for SDACC. By combining the
542   Equations 1 and 25:

$$\gamma_{SL} - \sigma_{SL} = \gamma_L \left(\kappa + \cos\theta_Y \right) \tag{52}$$

543   According to Equation 52, there is a difference between the interfacial energies measured on the
544   interfacial area solid-liquid (γ_{SL}) and on the contour line (σ_{LS}) solid-liquid-gas. This difference is controlled
545   by the liquid surface tension and by $\kappa + cos\theta_Y$. Figure 15 shows the behavior of this difference as a function
546   of Young's contact angle. According to this, the interfacial energy solid-liquid measured by Young's
547   model on the contour line is only valid for the solid-liquid interface in the case of complete wetting (θ_Y =
548   0°).

549   By Young's model, complete wetting means $\gamma_S = \sigma_{LS} + \gamma_L$, because the contact angle is zero ($cos\theta_Y$ = 1).
550   In this wetting case, SDACC predicts κ = -1, which leads to $\gamma_S = \gamma_{LS} + \gamma_L$. According to this, at complete
551   wetting both models match, ie. $\gamma_{SL} = \sigma_{LS}$.

552   At the opposite end, by θ_Y = 180° ($cos\theta_Y$ = -1), the Young's model predicts that $\gamma_S = \sigma_{LS} - \gamma_L$, that means
553   that $\sigma_{LS} = \gamma_L$, because, by definition, γ_S is zero by non-wetting. By SDACC, non-wetting means that κ tends
554   to one (see Figure 14). While in this case, γ_S tends to zero, then γ_{SL} tends to γ_L (see Eq. 25), practically in
555   agree with Young`s wetting model.

556   As can be seen, SDACC and Young`s model agree at the limits of complete wetting and non wetting.
557   However, both models predict quite different behaviors among these limits. These differences can be
558   quantified by $\kappa + cos\theta_Y$ (see the red curve in Figure 15), that, multiplied by the surface tension of the liquid
559   (see Eq. 52) results in the difference between the interfacial energy solid-liquid measured on the interface
560   (γ_{SL}), and on the contour line (σ_{LS}).
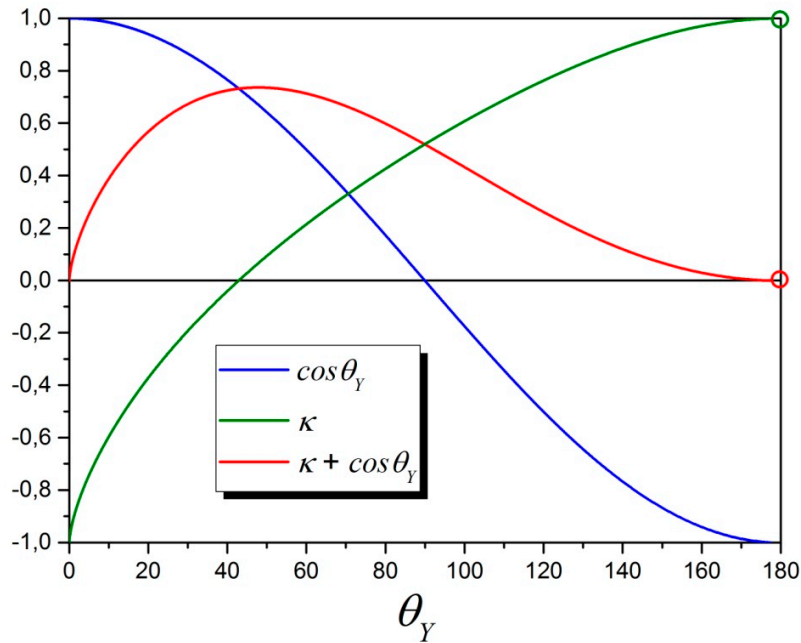
561   **Figure 15.** Comparison between the relevant parameters of Young's model and the SDACC model.

562   As mentioned above, by Young's model, at $\theta_Y = 90°$ the surface energy of the solid equals the tensor
563   solid-liquid on the contact point, ie., $\sigma_{SL} = \gamma_S$. This point represents the transition hydrophilic-hydrophobic
564   by Young's model. Instead, by SDACC, the case $\gamma_{SL} = \gamma_S$ occurs when $\kappa = 0$, at $\theta_Y = 42.88°$. In this case, the
565   area of the liquid-air interface at the equilibrium is the same as before starting the wetting process (Ω_L
566    $= \Omega^o$). Indeed, this can occur only if the energy of the solid-air interface is the same of the energy of the
567   solid-liquid interface. As already mentioned, this would represent the transition hydrophobic-hydrophilic
568   by using the SDACC model. This wetting threshold could also help to explain why the microgravity
569   decreases the contact angles of all the polymer surfaces that have contact angles lower than 90 degrees but
570   higher than 42.88 degrees. Those surfaces are, according to the SDACC, still hydrophobic ($\gamma_S < \gamma_{SL}$). But, if
571    $\kappa' < 0$, then $\theta_{\kappa'} < 42.88°$, and $\gamma_S > \gamma_{SL}$, according to Equation 25. This condition -the hydrophilicity by
572   SDACC- would increase wetting easily by applying a gravitational force and, in consequence, decrease
573   considerably the contact angle, see the explanation of Figure 16. New tests using hydrophilic surfaces
574   with contact angles lower than 42.88 degrees need to be realized in the future to probe this hypothesis.
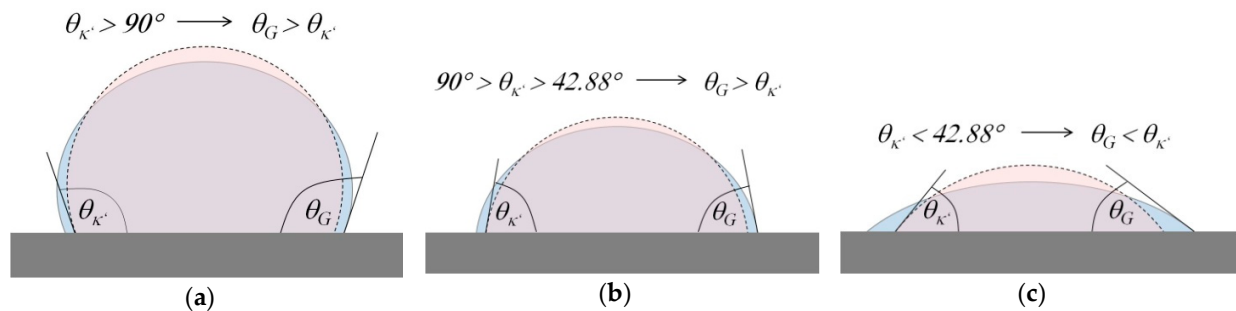575

576   **Figure 16.** The effect of gravity on the contact angle depends on the value of κ', which defines the threshold
577        $\theta_{\kappa'} = 42.88°$. (**a**) and (**b**) represent the case $\kappa' > 0$. The case (c) occurs if $\kappa' < 0$. Only in this case the gravity
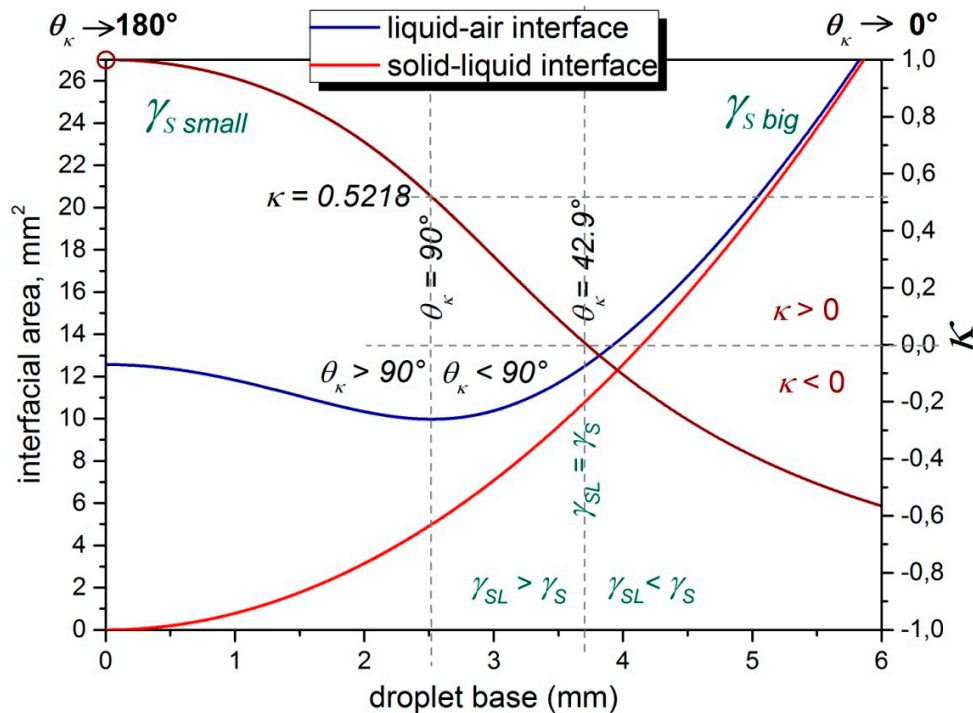578   leads to a smaller contact angle than the microgravity.

22

Figure 17. Relevant parameters of SDACC for a 1 mm radius droplet that wets a smooth surface.

All the contrasts between Young's model and SDACC mentioned so far are the result of using two completely different thermodynamic concepts. In the first case, the energetic balance is applied on the contour line solid-liquid-gas, while in the second case, on all the interfacial areas of the system. Figure 17 is a diagram of the SDACC-parameters for any system consisting of a 1 mm radius droplet of any liquid on any smooth solid surface.

6. Conclusion

A new method for the surface characterization, the Sessile Drop Accelerometry (SDACC), was studied and discussed using new experimental data. This method can measure the interfacial solid-gas and solid-liquid energies by submitting a sessile drop to uniform and controlled microgravity environment using a small acceleration tower designed for the use inside the laboratory.

The method bases on the thermodynamic equilibrium of the interfaces and not on the balance of bi-dimensional tensions on the contour line and, in consequence, does not follow Young's equation, as the current surface wetting characterization techniques usually do. For that reason, the measurement of the apparent contact angles is not a requirement for the application of SDACC.

The experimental results of seven different smooth polymer surfaces were compared with the measurements using the conventional methods of Owens et al. and Wu. The results show that SDACC provides similar values of the obtained by Owens et al. with good reproducibility. The effect of the receding wetting during the experiment and its implication on the results was also discussed.

For the application of the method, only one liquid with a known value of surface tension is needed. The values of the interfacial energies can be obtained by solving a linear system of two equations. No correlations or numerical methods are needed. The greatest obstacle to the method accuracy is the vibration produced during the start of the wetting process. However, the experimental results are showing that the release of these vibrations occurs for a very short time and could help the receding wetting. The high-speed camera of the instrument allows obtaining images of the droplets for an additional time free of vibrations.

The thermodynamic model that supports SDACC allows to measure the interfacial solid-liquid energy directly and not only the value of the tensor in the solid-liquid-air contour line. This is the most important advantage of SDACC over Young's equation based methods. The second important advantage is to allow the study of wetting phenomena without the effect of the terrestrial gravity.

In contrast to the universally accepted boundary wetting threshold of 90 degrees (Young's model), the thermodynamic model of SDACC proposes that the surface wetting threshold between hydrophobic and hydrophilic characters occurs when the contact angle on the drop boundary is 42.88 degrees ($\gamma_{SL} = \gamma_S$). This is probably the most challenging proposal of SDACC.

The instrument and its evaluation method open new possibilities to develop surface characterization procedures by submitting the solid-liquid-system to artificial generated and uniform force fields.

Conflicts of Interest: The author declares no conflict of interest.

References

1. Young, T. An Essay on the Cohesion of Fluids. *Phil. Trans. R. Soc. Lond.* **1805**, 95, 65-87

2. Sheng, Y. J.; Shaoyi, J.; Tsao, H. K. Effects of geometrical characteristics of surface roughness on droplet wetting. *The Journal of Chemical Physics* **2007**, 127, 23, 4704-7

3. Gibbs, J. W. *The Scientific Papers of J. Willard Gibbs, Thermodynamics* vol 1. Dover Publications, New York, 1961

4. Whyman, E.; Bomarschenko, G.; Stein, T. The rigorous derivation of Young, Cassie-Baxter and Wenzel equations and the analysis of the contact angle hysteresis phenomenon. *Chem. Phys. Lett.* **2008**, 450, 355-359

5. Roura, P.; Fort, J. Local thermodynamic derivation of Young's equation. *J. Colloid Interface Sci.* **2004**, 272, 420-429

6. Makkonen, L. Young's equation revisited. *J Physics.: Condens Matter* **2016**, 288, 135001

7. Orowan, E. Surface energy and surface tension in solids and liquids. *Proc. R. Soc. A* **1970**, 316 473-91

8. Bikerman, J. Surface energy of solids.*Top. Curr. Chem.* **1978**, 77 1-66

9. Ivanov, I. B.; Kralchevsky, P. A.; Nikolov, A. D. Film and Line Tension Effects on the Attachment of Particles to an Interface. *J. Colloid Interface Sci.* **1986**, 112 97-107

10. Makkonen, L. Misinterpretation of the Shuttleworth equation. *Scr. Mater.* **2012**, 66, 627-9

11. Makkonen, L. Misconceptions of the Relation between Surface Energy and Surface Tension on a Solid. *Langmuir* **2014**, 30 (9), 2580-2581

12. Gao, L.; McCarthy, T. J. An Attempt to Correct the Faulty Intuition Perpetuated by the Wenzel and the Cassie "Laws" *Langmuir* **2009**, 25 (13), 7249-7255

13. Gao, L.; McCarthy, T. J. Wetting 101° *Langmuir* **2009**, 25(24), 14105-14115

14. Hawa, T.; Zachariah, M. R. Internal pressure and surface tensión of bare hydrogen coated silicon nanoparticles. *J. Chem. Phys*. **2004**, 121(18), 9043-9049

15. Chu, K. H.; Xiao, R.; Wang, E. N. Uni-directional liquid spreading on asymmetric nanostructured surfaces. *Nat. Mater.* **2010**, 9, 413-417

16. Malvadkar, N. A.; Hancock, M. J.; Sekeroglu, K.; Dressick, W. J.; Demirel, M. C. An engineered anisotropic nanofilm with unidirectional wetting properties. Nat. Mater. 2010, 9 (12),1023-1028

17. Liu, Y.; Wang, J.; Zhang, X. *Sci. Rep.* **2013**, 3, 2008

18. Bico, J.; Roman, B.; Moulin, L.; Boudaoud, A. Adhesion: Elastocapillary coalescence in wet hair. *Nature* **2004**, 432, 690

19. Leger, L.; Joanny, J. F. Liquid spreading. *Rep. Prog. Phys.* **1992**, 55, 431-486

20. Fujii, H.; Nakae, H. Effect of gravity on contact angle. *Philosophical Magazine A* **1995**, vol. 72, Issue 6

21. Ababneh, A.; Amirfazli, A.; Elliott, J. A. Effect of Gravity on the Macroscopic Advancing Contact Angle of Sessile Drops. *The Canadian Journal of Chemical Engineering* **2006**, 84, 39-41

22. Diana, A.; Castillo, M.; Brutin, D.; Steinberg, T. Sessile Drop Wettability in Normal and Reduced Gravity. *Microgravity Sci. Technol.* **2012**, 24, 195-202

23. Zhu, Z-Q.; Wang, Y.; Liu, Q-S.; Xie, J-C. Influence of Bond Numbers on Behaviors of Liquid Drops Deposited onto Solid Substrates. *Microgravity Sci. Technol.* **2012**, 24, 181-188

652 24. Allen, J.S. An analytical solution for determination of small contact angles from sessile drops of arbitrary size.
653   *Journal of Colloid and Interface Science* **2003**, 261**,** 481-489

654 25. Neumann, A. W.; Li, D. Equation of State for Interfacial Tensions of Solid-Liquid Systems. *Advances in Colloid and*
655   *Interface Science* **1992**, 39, 299-345

656 26. Hejda, F.; Solar, P.; Kousal, J. Surface Free Energy Determination by Contact Angle Measurements – A
657   Comparison of Various Approaches. *WDS'10 Proceedings of Contributed Papers Part III* **2010**, 25-30

658 27. Fox, H. W.; Zisman, W. A. The spreading of liquids on low energy surfaces. *J. Colloid Sci.* **1950**, 5, 514-531

659 28. Owens, D. K.; Wendt, R. C. *Estimation of the Surface Free Energy of Polymers* **1969**, 13 1741-1747

660 29. Janczuk. B.; Bialopiotrowicz, T. Surface Free-Energy Components of Liquids and Low Energy Solids and Contact
661   Angles. *J. Colloid Interface Sci.* **1989**, 127, 189-204

662 30. Wu, S. Calculation of Interfacial Tension in Polymer Systems. *J. Polymer Sci.* Part C **1971**, 34, 19-30

663 31. van Oss, C. J.; Chaudhury, M. K.; God, R. J. Monopolar Surfaces. *Adv. Colloid Interface Sci.* **1987**, 28, 35-64

664 32. Kwok, D. Y. et al. Low-Rate Dynamic Contact Angles on Polystyrene and the Determination of Solid Surface
665   Tensions. *Polymer Eng. Sci.***1998**, 38, 1675-1684

666 33. Shimizu, R. N.; Demarquette, N. R. Evaluation of Surface Energy of Solid Polymers Using Different Models.
667   *Appl. Polym. Sci.* **2000**, 76 1831-1845

668 34. Chibowski, E. et al. Surface Free Energy Components of Glass from Ellipsometry and Zeta Potential
669   Measurements. *J. Colloid Interface Sci.* **1989**, 132 54-61

670 35. Calvimontes, A.; The Measurement of the Surface Energy of Solids using a Laboratory Drop Tower, *npj*
671   *Microgravity*, DOI **10.1038/s41526-017-0031-y**, 2017

672 36. Andrade, J. D.; Smith, L. M.; Gregonis, D. E. Surface and Interfacial Aspects of Biomedical Polymers. *Springer US*
673   2005, 249-292

674 37. Myers, D. Surfaces, Interfaces and Colloids: Principles and Applications. *John Wiley & Sons, Inc*. 2002, 19-23

675 38. Johnson, R. E.; Dettre, R. H. Contact Angle Hysteresis. Advances in Chemistry **1964**, vol. 43 112-135

676 39. Brandon, S.; Marmur, A. Simulation of Contact Angle Hysteresis on Chemically Heterogeneous Surfaces. *J.*
677   *Colloid Interface Sci*. **1996**, 183 351-355

678 40. Grundke, K. Handbook of Applied Surface and Colloid Chemistry. *John Wiley & Sons, Ltd.* 2001

679 41. Lubarda, V. A.; Talke, K. A. Analysis of the Equilibrium Droplet Based on an Ellipsoidal Droplet Model.
680   *Langmuir* **2011**, 27**,** 10705-10713

681 42. Whyman, G.; Bormashenko, E. Oblate spheroid model for calculation of the shape and contact angles of heavy
682   droplets. *Journal of Colloid and Interface Science* **2009**, 331 174-177

683 43. Keisan Online Calculator. Available online: http://keisan.casio.com/exec/system/1223382199 (accessed on 10
684   August 2017)

685 44. Keisan Online Calculator. Available online: http://keisan.casio.com/exec/system/13581717527 (accessed on 10
686   August 2017)

687 45. Educational Brief of the National Aeronautics and Space Administration. Available online:
688   https://er.jsc.nasa.gov/seh/microgravity_drops.pdf (accessed on 10 August 2017)

689 46. DRL School Lab. Available online: http://www.dlr.de/schoollab/en/desktopdefault.aspx/tabid-7474/12599_read-
690   31090/ (accessed on 10 August 2017)

691